Desalination and Water Treatment
www.deswater.com

doi: 10.5004/dwt.2023.29488

291 (2023) 32–43
April

Energy, exergy and economic assessments of novel sustainable solar powered evacuated tube collector integrated active desalination system

Angesh Kumar Shukla[a], Prashant Saini[a,*], Azharuddin[a], Vijay Kumar Dwivedi[b]

[a]*Department of Mechanical Engineering, Madan Mohan Malaviya University of Technology, Gorakhpur, UP 273010, India, Tel.: +91-9235552360; email: psme@mmmut.ac.in (P. Saini)*
[b]*Training and Placement Cell, Madan Mohan Malaviya University of Technology, Gorakhpur, UP 273010, India*

Received 5 November 2022; Accepted 18 March 2023

ABSTRACT

Novel sustainable solar powered combined desalination and hot water system is investigated based on energy, exergy and economic performances experimentally. For the purpose, evacuated tube collector integrated serpentine based active desalination unit is fabricated to fulfil the potable water and hot water supply especially in hospitals, hill station buildings and remote locations. Experimental investigations are performed for various mass flow rates in serpentine at different basin water depth (0.03, 0.04 and 0.05 m) over nine typical days. Effect of solar insolation and atmosphere temperature on potable water yield and system energy and exergy efficiencies are analyzed under real weather conditions. Measurements reveal that, maximum daily potable water yield, energy efficiency, exergy efficiency and hot water temperature are obtained as 5.10 kg/m^2·day, 42.39%, 4.45% and 67°C, respectively at 0.03 m water depth and lower mass flow rate. Additionally, potable water cost per litre (CPL) found minimum as 0.04073 $/L/m^2 for 25 y of operating life of system.

Keywords: Energy and exergy; Economics; Solar energy; Evacuated tube collector; Active desalination system

1. Introduction

Earth has limited amount of drinking water availability even though over two-third of its exterior is water-covered. World-wide growth in population, industrialization and urbanization pollutes drinking water resources which causes various health issues. Potable water demand in the world is increasing day by day. Even now developed and developing countries are fossils dependent to produce drinking water, which causes global warming, fossil depletion and pollution (air and water). Energy security and sustainability, potable water and pollution are the world-wide challenges currently. Due to fossils price hike and environmental safety, renewable driven desalination systems are advantageous over conventional desalination systems. Solar energy (cost-free, clean, reliable and environment-friendly) driven desalination systems are better option to produce drinking water, where electricity is not available yet [1]. Electricity consumed desalination such as multistage flash distillation, vacuum distillation, vapor compression, electrolysis, multi-effect distillation and reverse osmosis techniques are disadvantageous over solar driven desalination (solar stills) technique to install at isolated islands, remote cold locations [2]. The conventional fuel driven energy generation system leads to negative environmental effects. Shahzad et al. [3] reviewed the current status of conventional desalination and power generation in contrast with environment protection and suggested hybridization of such systems with renewable energy for sustainable development and energy saving. Potable water and hot water are required in domestic applications like bathing, cleaning, cooking and in hospitals for washing equipment's and de-infect in contrast with current epidemic situation generated by corona virus. Shahzad et al. [4] evaluated the water production rate of a hybrid multi-effect

* Corresponding author.

distillation system integrated with adsorption cycle theoretically. Ng et al. [5] discussed the recent advancements in conventional distillation systems and recommended that hybridization of multi-effect distillation (MED) system with adsorption cycle (MEDAD) improves the production rate and thermal performances. Shahzad et al. [6] investigated the water production rate of MEDAD hybrid distillation system experimentally and found improved distillate than conventional MED. The distillation yield and thermodynamic performance of evacuated tube collector integrated different types of desalination system have been reviewed by Kumar et al. [7]. In addition, possible suggestions to improve the desalination system performances have been presented by Chhabra et al. [8]. Considering this, solar desalination system including heating effect is current research need to produce hot water and drinking water supply demand especially at arid areas, remote locations and hills stations. Researchers worked on enhancing performance of solar still by changing their geometries, combinations and arrangements.

The different design of direct and indirect solar desalination methods has been exhaustively reviewed and recommended indirect methods for medium and large-scale whereas direct methods for small scale desalination [9]. Manokar et al. [10] reviewed photovoltaic collector integrated different solar stills and summarised that photovoltaic module do not affect the stills distillation yield while they can be used to improve the overall system efficiency. Singh et al. [11] reviewed different design of solar driven passive distillers based on their productivity, efficiency and economy. Tiwari and Tiwari [12] analyzed the seasonal and annual performance of single slope passive solar still at different water depth and revealed that the distillation yield was higher at lower water depth. Kabeel et al. [13] assessed the distillation yield of external condenser integrated passive solar still using aluminium-oxide nanoparticle in basin water. Sharshir et al. [14] enhanced the distillation yield of solar still using various nanoparticle concentrations and studied the effects of different basin water depth and glass cover cooling. Shanmugan and Essa [15] investigated daily productivity and energy efficiency of nanoparticles coated basin liner passive solar still for a typical summer and winter day by both theoretically and experimentally. Singh et al. [16] investigated the effect of mass flow rate on distillation yield and thermal performances of solar collector integrated SSSS. Kumar et al. [17] analyzed the effects of mass flow rate and collectors on thermal performances of an active desalination system. Thermodynamic performance and sensitivity analysis of solar-driven single slope desalination system considering the effect of number of similar evacuated tube collector (ETCs) in series experimentally [18,19]. Sandeep et al. [20] examined the daily distillation yield of flat plate collector integrated single basin active desalination unit considering different condensing surface material, shading and basin water depth experimentally. Singh et al. [21] examined thermodynamic performance of single slope active desalination unit integrated with evacuated collector at different water depth over the day. Sampathkumar et al. [22] compared the distillation yield and performance index of single basin single slope passive and active desalination system at different water mass. Kumar et al. [23] investigated daily productivity, performance index and exergetic efficiency of ETC augmented single slope single basin desalination system under forced circulation mode. Joshi and Tiwari [24] compared the energy and exergy efficiencies and CPL of potable water for three different systems under different climate conditions. Sharma et al. [25] investigated the enviroeconomic and exegoeconomic performances of solar collector integrated single slope solar still. Moreover, researchers are more interested towards double slope active solar stills nowadays.

Sharshir et al. [26] discussed the theoretical approach to evaluate the potable water productivity and energy and exergy performances for modified passive and active desalination system. Yadav et al. [27] simulated the daily productivity and energy and exergy efficiencies of double slope solar still (DSSS) integrated with evacuated tube solar collector using MATLAB. Dwivedi and Tiwari [28] evaluated the performances of single and double slope passive desalination systems at different water depth under winter and summer climates. Rajaseenivasan and Murugavel [29] evaluated the performance of double basin double slope passive desalination system at various water level in lower and upper basin. Elango and Murugvel [30] evaluated the performances of double slope single and double basin passive solar still for different water depth and insulation on basin and obtained higher productivity at lower water depth. Singh et al. [31] investigated distillation output, thermal and economic performances of single and double slope passive desalination systems. Sahota and Tiwari [32] estimated the distillation yield of passive double slope solar still (DSSS) for different water mass in the basin with and without nanoparticle theoretically. Jani and Modi [33] experimentally evaluated the effects of different cross section of fins with different water depth for passive DSSS and revealed that the productivity was higher at lower water depth with circular cross section fins. Dwivedi and Tiwari [34] examined the hourly distillation yield, energy and exergy efficiencies of active DSSS considering natural circulation mode. Singh et al. [35] designed hybrid PV collector coupled DSSS under both forced and natural circulation mode and examined daily distillation rate and performance index. Morad et al. [36] examined the performance of flat-plate solar collector integrated double slope active and passive solar still with and without glass cover cooling and found higher productivity for active solar still with glass cover cooling. Kumar et al. [37] studied the effect of water depth on distillation yield and thermal performance of DSSS integrated with photovoltaic collectors. Fathy et al. [38] compared the performance of three different arrangements of parabolic trough collector (PTC) integrated DSSS for different water depth in both summer and winter season experimentally. Mohammadi et al. [39] evaluated the productivity and energy performance of PTC integrated active DSSS for different heat exchangers design in basin experimentally. Hedayati et al. [40] evaluated distillation yield and thermodynamic performances of photovoltaic collector integrated DSSS with phase change material in still basin for different water mass. Tiwari et al. [41] designed the photovoltaic and compound parabolic collector integrated active desalination unit and analyzed the effect of mass flow rate, inclination angle of condensing cover and packing factor on distillation yield and thermodynamic performance. Singh and Tiwari [42] compared the distillation yield and energy and exergy efficiencies of photovoltaic and compound parabolic collector

driven single and double slope active desalination system. Raturi et al. [43] examined the distillation yield and thermal efficiency of DSSS including compound parabolic collector integrated with ETC. Singh et al. [44] investigated the effect of mass flow rate on year-round thermal performances of DSSS integrated with solar compound parabolic collectors. Deniz and Cinar [45] designed novel solar-driven humidification and dehumidification desalination system and investigated thermodynamic, environmental and economic performances. Rahbar et al. [46] compared the performances of two novel desalination system considering effects of atmospheric temperature and solar insolation theoretically as well as experimentally. Kabeel et al. [47] designed two novel desalination systems incorporating composite and phase change materials as heat storage and compared the economic and thermodynamic performances. Mosleh et al. [48] examined energy and economical performances for combined evacuated tube and parabolic trough collectors integrated desalination system experimentally and improved the distillation yield. Singh [49] evaluated the distillation yield, exergy and economic performances of identical ETC integrated active DSSS theoretically. Singh et al. [50] investigated the effect of mass flow rate on productivity, exergy, economic and enviro-economic parameters of DSSS integrated with photovoltaic compound parabolic collectors. Dubey et al. [51] investigated thermodynamic and economical performances for parallel ETC integrated DSSS desalination system under forced mode theoretically.

According to above reviewed literatures, scanty research reported related to sustainable solar powered combined desalination and hot water (CDHW) system so far, that could be beneficial and attractive especially at hill stations, hospitals and remote buildings. In addition, solar driven serpentine based active desalination system has not been evaluated yet experimentally. In current research, solar collector integrated with serpentine based double slope active desalination system powered by solar energy is investigated experimentally. For the purpose, ETC integrated active DSSS is fabricated on the roof of Madan Mohan Malaviya University of Technology, Gorakhpur, India. The data of solar intensity and ambient temperature are recorded for 9 days (03–11 March) at Gorakhpur, India. Proposed system is analyzed based on energy, exergy and economic performances. Convection, evaporation and radiation heat transfer coefficients are calculated based on recorded inner glass surface and basin water temperatures. Further, hourly water productivity and overall energy and exergy efficiencies of the system are evaluated. Eventually, the cost per litre of potable water is compared for different operating years of the system.

2. System description

Proposed combined desalination and hot water system utilizes solar insolation, which is free of cost, environment friendly and in abundant availability while conventional systems utilize fossils (depleting drastically and polluting environment). Solar driven desalination systems (solar stills) are advantageous over electricity driven conventional systems (vapor compression, electrolysis and reverse osmosis). This system is designed especially for hill stations, cold remote locations and roofs of building where electricity is not available yet. Evacuated tube collector frequently works in the windy, cloudy and cold days. ETC efficiency is higher due to higher operating temperature (up to 200°C) than flat plate collectors.

Fig. 1a and b illustrate the ETC integrated DSSS experimental set-up and top view of DSSS, respectively. Proposed system is fabricated and installed at Madan Mohan Malviya University of Technology, Gorakhpur, (latitude 26.76°N, longitude 83.37°E) India. Main components of system are water tank, evacuated tubes, header, frame, stand and DSSS. The collector unit is incorporated with polyurethane foam insulated header, in which a copper pipe heat exchanger is embedded. ETC tubes are mounted on frame at an inclination of 27° with horizontal and facing due south for maximum absorption of falling solar insolation. Serpentine based double slope active desalination unit is fabricated with locally available materials and coupled with collector unit. The still basin is made up of 18-mm-thick plywood and a black painted galvanized iron sheet box is fitted inside it. The top of still basin is covered with 3 mm thick glass with 27° inclination. PVC pipes are fitted at both the lower ends of glass

Fig. 1. (a) Evacuated tube collector integrated double slope solar still experimental set-up. (b) Top view of double slope solar still.

for smooth flow of distilled water condensing inner side of glass to potable water container. The serpentine is installed at the bottom of still basin with 10° inclination from its inlet to outlet for smooth flow of working fluid. Silicone sealant and m-seal are used to make the system leak proof. Water is used as working fluid inside the ETC as well as serpentine circuit of experimental setup. Water tank, header and still serpentine are connected through polyolefin foam insulated PVC pipes. To measure the header inlet and outlet, serpentine inlet and outlet, basin water, still basin and glass inner and outer temperatures K-type thermocouples are inserted into the holes provided in PVC pipes and solar still. These thermocouples are connected to a digital temperature indicator through thermocouple wires. Solar energy absorbed by ETC tubes is transferred to working fluid inside it and gets heated up. The heated fluid moves in upward direction due to thermosyphon effect and gets converted into steam in header, where heat transfer occurs between steam and water coming from water tank. This heated water goes to DSSS serpentine through piping and transfers its heat energy to still basin water. The water coming out from still serpentine is collected in an insulated water tank and can be used for hot water supply. Basin water also absorbs the heat energy by still glass cover (transmitting solar energy) along with serpentine. Evaporation starts after reaching a certain temperature where saturated partial pressure of water is less than the partial pressure of water vapour. Evaporated water vapour gets condensed at inner glass surface by releasing its latent heat of condensation. Finally, this condensed water is collected in potable water container through PVC pipes fitted at both lower ends of glass cover. Technical details of experimental setup are presented in Table 1.

3. Mathematical equation

Mathematical equations are presented to investigate system energy efficiency, exergy efficiency and economic performance of proposed active desalination and hot water system. There are two main sub-systems namely collector and double slope solar still. The evaporative loss and side heat loss are neglected and water level in still basin is kept constant.

3.1. Energy analysis

Energy analysis is done to investigate ETC, active solar still and overall system energy efficiencies. Energy input, useful energy gain and energy efficiency of ETC are given as [52]:

$$Q_{\text{in,sun,ETC}} = I_t \times A_p \tag{1}$$

$$Q_u = \dot{m}_w c_{\text{pw}} \left(T_{\text{out}} - T_{\text{in}}\right) \tag{2}$$

$$\eta_{I,\text{ETC}} = \dot{m}_w c_{\text{pw}} \frac{\left(T_{\text{out}} - T_{\text{in}}\right)}{Q_{\text{in,sun,ETC}}} \tag{3}$$

The energy utilized by solar still is given as:

$$Q_{u,\text{SS}} = h_{\text{ew}} A_b \left(T_{\text{sw}} - T_{\text{gi}}\right) \tag{4}$$

Evaporation, convection and radiation heat transfer coefficients are determined as [34]:

$$h_{\text{ew}} = 0.016273 \times h_{\text{cw}} \times \left(\frac{P_w - P_{\text{gi}}}{T_{\text{sw}} - T_{\text{gi}}}\right) \tag{5}$$

$$h_{\text{cw}} = 0.884\left[\left(T_{\text{sw}} - T_{\text{gi}}\right) + \frac{\left(P_w - P_{\text{gi}}\right)\left(T_{\text{sw}} + 273\right)}{\left(268900 - P_w\right)}\right]^{1/3} \tag{6}$$

$$P_w = \exp^{\left(25.317 - \frac{5144}{T_{\text{sw}} + 273}\right)} \tag{7}$$

$$P_{\text{gi}} = \exp^{\left(25.317 - \frac{5144}{T_{\text{gi}} + 273}\right)} \tag{8}$$

$$h_{\text{rw}} = \varepsilon_{\text{eff}} \times \sigma\left(T_{\text{sw}} + T_{\text{gi}} + 546\right)\left[\left(T_{\text{sw}} + 273\right)^2 + \left(T_{\text{gi}} + 273\right)^2\right] \tag{9}$$

$$\frac{1}{\varepsilon_{\text{eff}}} = \frac{1}{\varepsilon_w} + \frac{1}{\varepsilon_g} - 1 \tag{10}$$

where ε_w and ε_g are the emissivity of water and glass cover, respectively. Energy input through sun and serpentine to the solar still can be evaluated as, respectively:

$$Q_{\text{in,sun,SS}} = I_t \times A_b \tag{11}$$

$$Q_{\text{in,sp,ss}} = \dot{m}_{w,\text{sp}} c_{\text{pw}} \left(T_{\text{in,sp}} - T_{\text{out,sp}}\right) \tag{12}$$

Table 1
Technical details of experimental set-up

Parameter	Value
G.I. sheet thickness, mm	1
Plywood thickness, mm	18
Glass cover thickness, mm	3
Glass cover inclination	27°
Basin area, m^2	0.44
Glass cover area, m^2	0.49
Serpentine length, m	2.83
Serpentine inner diameter, mm	10
Serpentine outer diameter, mm	12
Storage tank capacity, L	200
Evacuated tubes	15
Evacuated tube inner diameter, mm	37
Evacuated tube outer diameter, mm	47
Evacuated tube length, mm	150
Effective area of evacuated tube collector, m^2	1.057
Insulation thickness of connecting pipes, mm	10
Insulation thickness of header, mm	30

Therefore, the active solar still energy efficiency is determined as:

$$\eta_{I,\mathrm{SS}} = \frac{Q_{u,\mathrm{SS}}}{Q_{\mathrm{in,sun,ss}} + Q_{\mathrm{in,sp,ss}}} \tag{13}$$

Moreover, the overall energy efficiency of combined desalination and hot water system is calculated as:

$$\eta_{I,\mathrm{overall}} = \frac{Q_{u,\mathrm{SS}}}{Q_{\mathrm{in,sun,ETC}} + Q_{\mathrm{in,sun,SS}}} \tag{14}$$

3.2. Exergy analysis

The exergy analysis is done to evaluate the evacuated tube collector, active solar still and overall system exergy efficiencies. The exergy input through the sun is given as [34]:

$$\dot{X}_{\mathrm{Sun}} = I_t A_p \left[1 - \frac{4}{3}\left(\frac{T_a + 273}{T_s} \right) + \frac{1}{3}\left(\frac{T_a + 273}{T_s} \right)^4 \right] \tag{15}$$

Where T_s is the temperature of Sun and taken as 4,500 K [53]. The exergy utilized and exergy efficiency of collector is given as:

$$\dot{X}_{u,\mathrm{ETC}} = \dot{m}_w c_{\mathrm{pw}} \left[\left(T_{\mathrm{out}} - T_{\mathrm{in}} \right) - \left(T_a + 273 \right) \ln\left(\frac{T_{\mathrm{out}} + 273}{T_{\mathrm{in}} + 273} \right) \right] \tag{16}$$

$$\eta_{\mathrm{II,ETC}} = \frac{\dot{X}_{u,\mathrm{ETC}}}{\dot{X}_{\mathrm{Sun,ETC}}} \tag{17}$$

The exergy utilized by the active solar still is determined as [34]:

$$\dot{X}_{u,\mathrm{SS}} = Q_{u,\mathrm{SS}} \left(1 - \frac{T_a + 273}{T_{\mathrm{sw}} + 273} \right) \tag{18}$$

Therefore, the active solar still exergy efficiency is determined as:

$$\eta_{\mathrm{II,SS}} = \frac{\dot{X}_{u,\mathrm{SS}}}{\left(\dot{X}_{\mathrm{Sun,SS}} + \dot{X}_{\mathrm{sp,SS}} \right)} \tag{19}$$

Moreover, the overall exergy efficiency of combined desalination and hot water system is calculated as:

$$\eta_{\mathrm{II,overall}} = \frac{\dot{X}_{u,\mathrm{SS}}}{\dot{X}_{\mathrm{Sun,ETC}} + \dot{X}_{\mathrm{Sun,SS}}} \tag{20}$$

3.3. Economic analysis

Economic analysis is done to determine the total cost of fabricated system and CPL of produced potable water. Capital recovery factor (CRF) is the main economic parameter expressed as:

$$\mathrm{CRF} = \frac{i\left(1+i\right)^N}{\left(1+i\right)^N - 1} \tag{21}$$

where interest rate (i) is assumed as 10% and system expected lifetime (N) is considered as 15, 20, and 25 y to compare CPL of produced potable water. Other important economic parameters associated with solar still modelling are salvage value (SV), capital investment (Z), sinking fund factor (SFF), fixed annual cost (FAC), annual cost (AC) annual salvage value (ASV) and annual maintenance cost (AMC). Salvage value is considered 10% of overall investment cost during the analysis [48,54]. All these economic parameters can be calculated as given in [53,54].

$$\mathrm{SV} = 0.1 \times Z \tag{22}$$

$$\mathrm{SFF} = \frac{i}{\left(1+i\right)^N - 1} \tag{23}$$

$$\mathrm{FAC} = \mathrm{CRF} \times Z \tag{24}$$

AMC is taken as 15% of FAC [54]. In this way, ASV and AC can be determined as respectively:

$$\mathrm{AMC} = 0.15 \times \mathrm{FAC} \tag{25}$$

$$\mathrm{ASV} = \mathrm{SV} \times \mathrm{SFF} \tag{26}$$

$$\mathrm{AC} = \mathrm{FAC} + \mathrm{AMC} - \mathrm{ASV} \tag{27}$$

$$M = \mathrm{DY} \times 365 \tag{28}$$

where DY is the daily yield (mass rate of evaporation in a day). Therefore, CPL of produced potable water of any system can be determined as:

$$\mathrm{CPL} = \frac{\mathrm{AC}}{M} \tag{29}$$

where M is the solar still annual yield.

3.4. Uncertainty analysis

The temperatures at various locations were recorded using thermocouples (*K*-type) integrated with digital temperature monitor. The ambient temperature was measured by mercury thermometer. A measuring jar was used to measure the potable water output from still. The solar intensity was measured with the help of pyranometer.

Two type of error sources occur generally to perform uncertainty analysis as random error (computed statistically through repeated observations) and systematic error (computed through information provided by manufacturer, calibration certificates and published literature). In this research, the uncertainty involved is systematic due to uniform distribution of all recorded data. The standard uncertainty is evaluated as [46]:

$$u = \frac{a}{\sqrt{3}} \tag{30}$$

where *a* and *u* represent the instrument accuracy and standard uncertainty, respectively. Table 2 shows the operating range, accuracy and standard uncertainty of various measuring instruments. The uncertainty of an output parameter (y) dependent on various input parameter (x_i) can be written as:

$$u(y)=\left[\left(\frac{\partial y}{\partial x_1}\right)^2 u^2(x_1)+\left(\frac{\partial y}{\partial x_2}\right)^2 u^2(x_2)+\ldots\right]^{1/2} \tag{31}$$

Thus, uncertainty associated with system hourly energy efficiency can be written as:

$$u(\eta)=\eta\left[\frac{u(\dot{m}_{ew})^2}{\dot{m}_{ew}^2}+\frac{u(I_t)^2}{I_t^2}\right]^{1/2} \tag{32}$$

Hence, maximum uncertainty for hourly system energy efficiency is obtained as 0.30%.

4. Results and discussion

The presented system performance depends on metrological parameter such as ambient temperature and solar insolation. The temperatures at different locations such as header inlet and outlet, basin water, basin liner, outer and inner glass are recorded in the system from 9–18 IST. Based on these recorded temperatures the convective, radiative and evaporative heat transfer coefficients are determined. The basin water depth and working fluid mass flow rate are considered as decision variables for assessment the system performance. The experiments are conducted for three different basin water depth as 0.03, 0.04 and 0.05 m with three different mass flow rates for each basin water depth. In this way total nine experiments on nine days (03–11 March) are carried out. The distillation yield, energy efficiency, exergy efficiency and cost per litre of potable water are the objective functions. Finally, the CPL of potable water is compared for different operating years of the system.

Fig. 2 shows the variation of solar intensity over the day. It is clearly observed that the radiation intensity continuously increasing before noon and reaches maximum at around 2 p.m. and finally decreases until end of the day. Fig. 3 shows the variation of ambient temperature over the day. The ambient temperature found maximum in between 1 to 2 p.m. for recorded days.

Table 2
Measuring instruments standard uncertainty

Measuring instrument	Range	Accuracy	Standard uncertainty
Thermometer	0°C–100°C	±1°C	0.6°C
Thermocouple	0°C–400°C	±1°C	0.6°C
Potable water pot	0–500 mL	±10 mL	5.8 mL
Pyranometer	0–2,500 W/m^2	±1 W/m^2	0.6 W/m^2

Figs. 4–6 show variation of inner glass surface and basin water temperatures for various water depths (0.03, 0.04, and 0.05 m) at three mass flow rates as 0.0013, 0.0027 and 0.0042 kg/s over the day, respectively. Figs. 4–6 show the

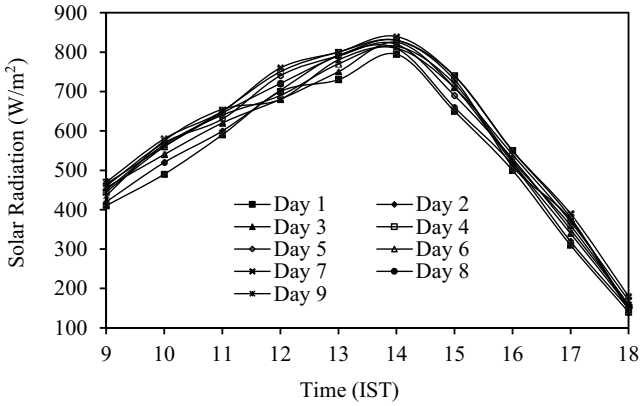

Fig. 2. Variation of solar intensity over the day.

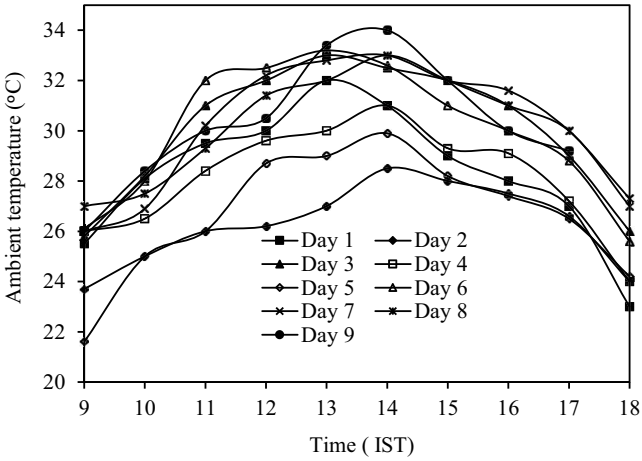

Fig. 3. Variation of ambient temperature over the day.

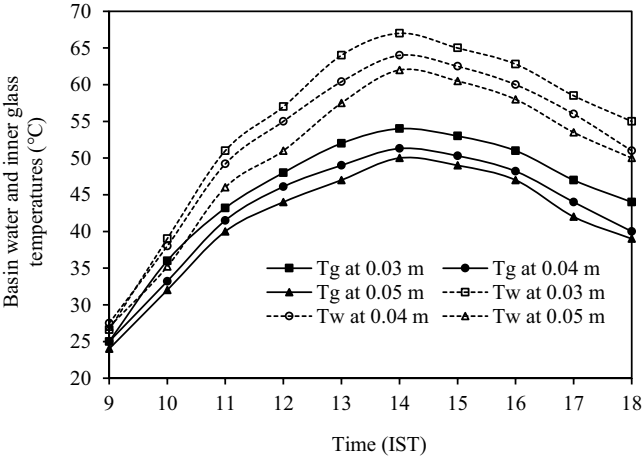

Fig. 4. Variation of basin inner glass and water temperatures for different water depths at flow rate 0.0013 kg/s over the day.

increasing trend of temperatures from morning to afternoon and reach its maximum value at around 2 p.m. and then start decreasing afterward. This is due to increase in solar radiation from the morning to early afternoon hours with the highest values attaining around 2 p.m. and then declining in late afternoon. The maximum recorded values of basin inner glass surface and water temperatures are 54°C and 67°C, respectively for 0.03 m water depth at 0.0013 kg/s mass flow rate. Measurement reveals that at a particular mass flow rate with increase in water depth both the basin water and inner glass temperature decreases, due to fact that more water mass in the basin requires more heat energy to elevate their temperatures. It is observed from Figs. 4–6 with increase in mass flow rate both inner glass temperature and basin water temperature are decreasing because at a higher mass flow rate the circulating fluid inside serpentine do not get enough time for heat transfer in header and hence still basin.

Figs. 7–9 show variation of radiation, convection and evaporation heat transfer coefficients for various water depth (0.03, 0.04, 0.05 m) at three mass flow rates as 0.0013, 0.0027 and 0.0042 kg/s over the day, respectively. At a perticular flow rate and water depth, it is observed that these three (radiative, convective and evaporative) heat transfer coefficients increase upto 2 p.m. and then decrease until sunshine of the day. These heat transfer coefficients are the function of basin water and inner glass temperatures, hence they follow same trends as these temperatures. Also, the increased basin inner glass and water temperatures increase saturated partial vapor pressure at water level more fastly than inner glass surface. In this way, the pressure difference between basin water and inner glass surface increases resulting in increased transpotation of molecules from water to inner glass surface. The maximum value of radiative, convective and evaporative heat transfer coefficients are obtained as 6.83, 2.75 and 41.23 W/m^2·K, respectively at 2 p.m. for water depth 0.03 m and flow rate 0.0013 kg/s. In overall, for a perticular mass flow rate with increse in basin water depth or vice-versa, these three heat transfer coefficients are decreasing.

Figs. 10–12 show the variation of hourly distillation yield and hot water outlet temperature for various water depth (0.03, 0.04, 0.05 m) at three mass flow rates as 0.0013,

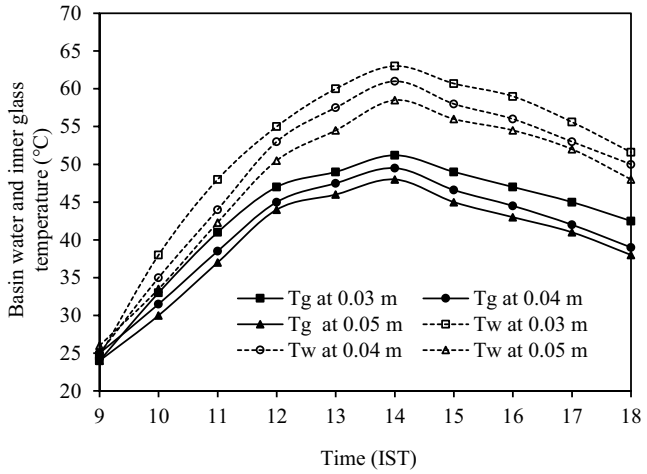

Fig. 5. Variation of basin inner glass and water temperatures for different water depths at flow rate 0.0027 kg/s over the day.

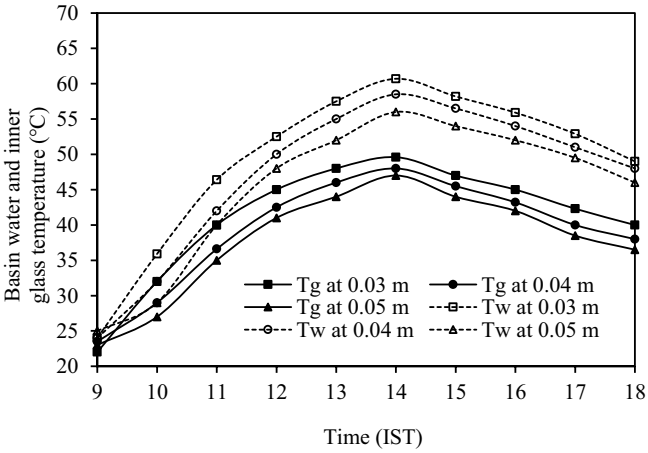

Fig. 6. Variation of basin inner glass and water temperatures for different water depths at flow rate 0.0042 kg/s over the day.

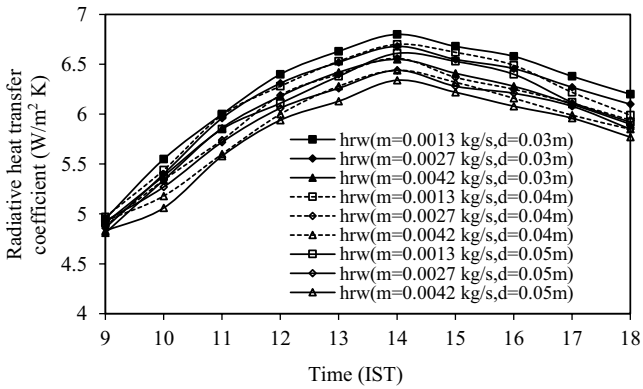

Fig. 7. Variation of radiative heat transfer coefficient for different mass flow rate and water depth over the day.

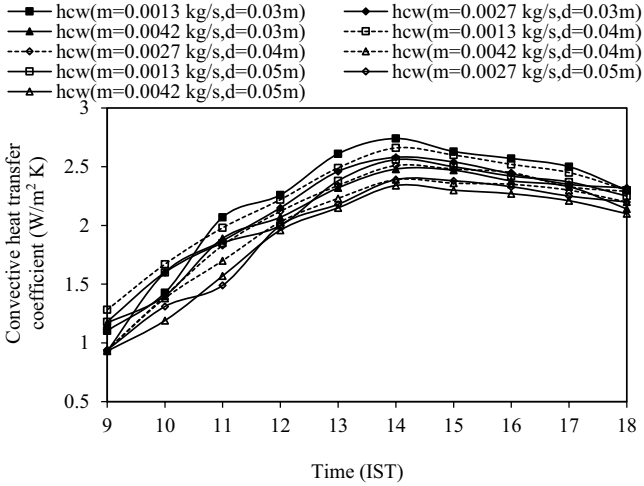

Fig. 8. Variation of convective heat transfer coefficient for different mass flow rate and water depth over the day.

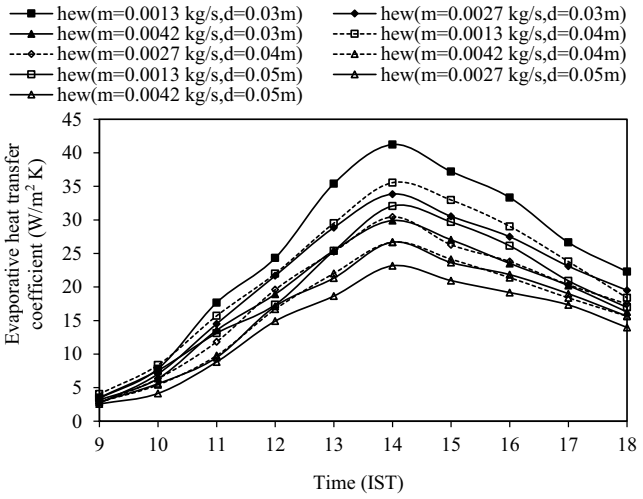

Fig. 9. Variation of evaporative heat transfer coefficient for different mass flow rate and water depth over the day.

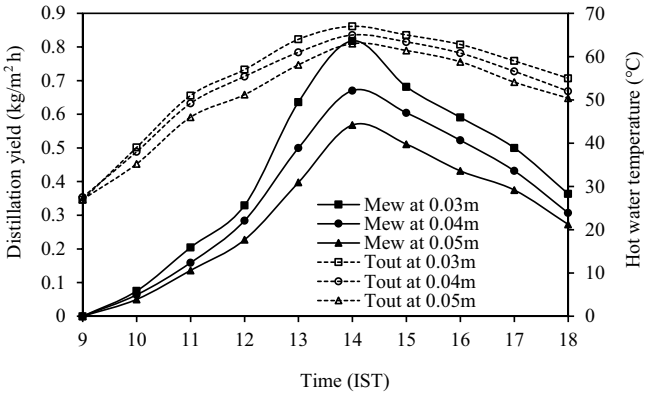

Fig. 10. Variation of hourly distillation yield and hot water temperature for different water depths at flow rate 0.0013 kg/s over the day.

0.0027 and 0.0042 kg/s over the day, respectively. At perticular mass flow rate it is seen that the hourly productivity and hot water outlet temperature decreases with increase in basin water depth. This occurs due to high thermal inertia effect of water in still basin. Measurement reveals that the mass flow rate have greater influence on hourly productivity and it decreases with increase in mass flow rate. Incresed mass flow rate reduces the time for heat exchange inside header and hence, still basin (between water flowing in serpentine and basin water). The maximum hourly productivity and hot water temperature are obtained as 0.818 kg/m^2·h and 67°C, respectively for 0.03 m water depth and 0.0013 kg/s mass flow rate. Moreover, experimental results indicate the least distillation yield during morning and late afternoon periods due to less heat addition to basin water. Also, the heat addition through ETC to solar still is less in morning and increases gradually till early afternoon hours. The hourly productivity is found maximum at around 2 p.m. due to maximum solar intensity.

Figs. 13–15 show variation of hourly system energy efficiency and exergy efficiency for various water depth (0.03,

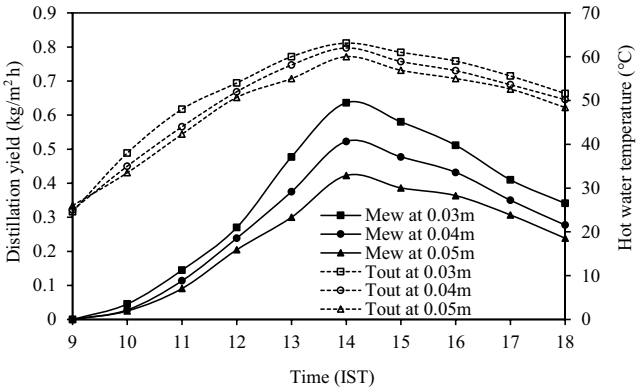

Fig. 11. Variation of hourly distillation yield and hot water temperature for different water depths at flow rate 0.0027 kg/s over the day.

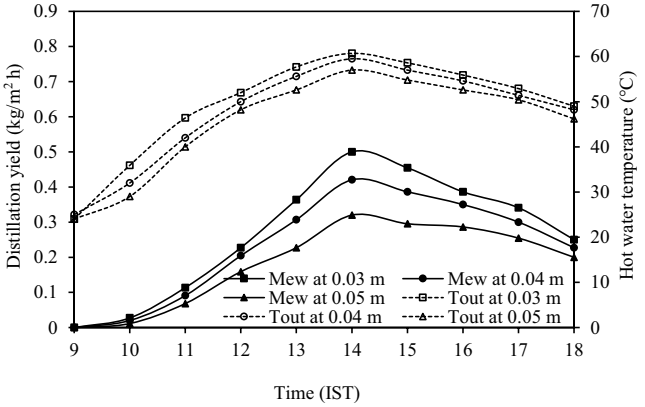

Fig. 12. Variation of hourly distillation yield and hot water temperature for different water depths at flow rate 0.0042 kg/s over the day.

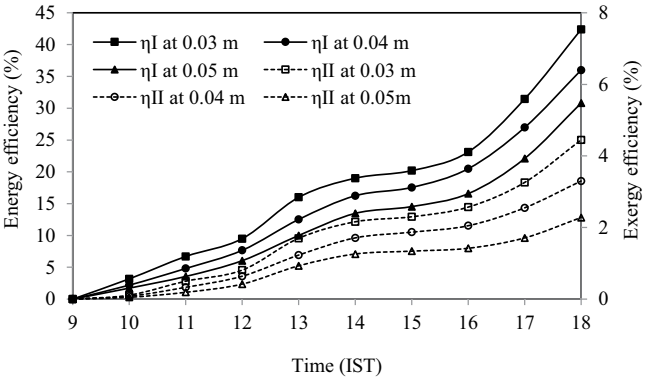

Fig. 13. Variation of hourly system energy and exergy efficiencies for different water depths at flow rate 0.0013 kg/s over the day.

0.04, 0.05 m) at three mass flow rates as 0.0013, 0.0027 and 0.0042 kg/s over the day, respectively. The hourly system energy and exergy efficiencies are increasing continuously from morning to till end of sunshine. The energy utilized increases more than energy input from morning to early

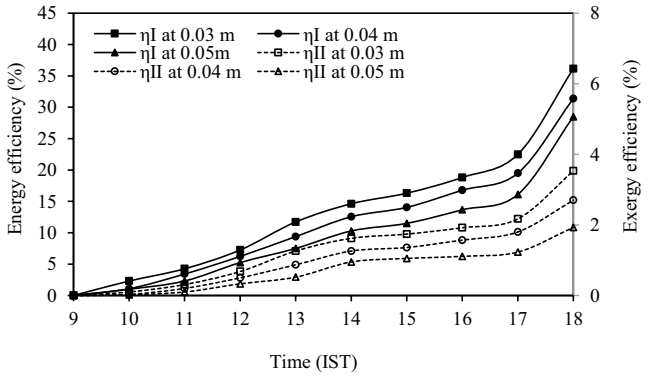

Fig. 14. Variation of hourly system energy and exergy efficiencies for different water depths at flow rate 0.0027 kg/s over the day.

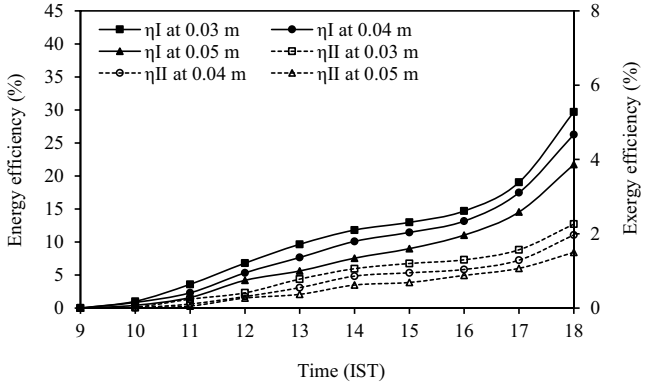

Fig. 15. Variation of hourly system energy and exergy efficiencies for different water depths at flow rate 0.0042 kg/s over the day.

afternoon after that energy input decreases rapidly than energy utilised resulting increased energy efficiency. Also, from morning to early afternoon evaporative exergy transfer increases at faster rate than input exergy, and after that evaporated exergy decreases slowly than exergy input resulting increased exergy efficiency. At a particular mass flow rate both energy and exergy efficiencies are reduced at higher water depth. It is due to fact that the basin water temperature decreases with increased water mass resulting decreased temperature difference between basin water and inner glass surface. The maximum hourly system energy and exergy efficiencies are found 42.39% and 4.45%, respectively for 0.0013 kg/s mass flow rate and 0.03 m water depth. In addition, the hourly system energy and exergy efficiencies are decreasing with increased mass flow rate due to less heat and exergy transfer through ETC and serpentine to basin water resulting decreased temperature difference between basin water and inner glass surface.

As the data for distillation yield is reported from 9–18 IST, whereas the daily yield and annual yield have been used for making calculations of potable water cost per litre. The potable water data for 18–9 IST is recorded for 9 days and found maximum as 1,100 mL. In this way, potable water data at lower water depth and mass flow rate along with maximum recorded out of 9 days makes daily yield. This daily yield is used to calculate the annual yield and fixed for system operation years. Keeping other parameters held fixed, only the number of operating years of the system are variable. Table 3 shows the cost of each component associated with the CDHW system including installation and testing. Results show that total capital investment and the average annual potable water production rate of proposed system are 627 US$ and 1,935 kg/m^2·y, respectively. Table 4 shows the comparison of CPL of potable water for different operating years (15, 20 and 25 y) of the system. To calculate the potable water cost per litre of system for different operating years, the economic modeling is simulated in Engineering Equation Solver (EES) package. The cost per litre of potable water is obtained minimum as 0.04073 $/L/m^2 for 25 y of operation.

Main features of proposed combined desalination and hot water production system can be written as follows: (i) It utilizes clean energy which is cost-free and reliable; (ii) It is simple in construction than traditional systems; (iii) It can

Table 3
Fabrication cost of combined desalination and hot water system

Item	Price ($)
Evacuated tube collector	350
Wooden stand	10
Wooden box	35
Glass cover	18
Copper serpentine	25
Measuring flask	5
Water tank	15
PVC pipe and valve	29
Galvanized iron box	22
Insulation and sealant material	28
Installation and testing	50
Labour charge	40
Total	627

Table 4
cost analysis of combined desalination and hot water system for different operating life

Parameter	Value		
Capital investment (*Z*), $	627		
Life of the solar still (*N*), y	15	20	25
Interest rate (*i*), %	10	10	10
Salvage value (*S*), $	62.7	62.7	62.7
Capital recovery factor (CRF)	0.1315	0.1175	0.1102
Sinking fund factor (SFF)	0.03147	0.01746	0.01017
Fixed annual cost (FAC), $	82.43	73.65	69.08
Annual salvage value (ASV), $	1.973	1.095	0.6375
Annual maintenance cost (AMC), $	12.37	11.05	10.36
Annual cost (AC), $	92.83	83.6	78.8
Annual yield (M), kg/m^2·y	1,935	1,935	1,935
Cost per litre (CPL), $/L/m^2	0.04798	0.04322	0.04073

fulfil the drinking water and hot water supply at small-scale; (iv) It saves environment and energy compared to electricity driven traditional systems; (v) It requires minimum capital investment cost. Hence, proposed CDHW system is recommended to generate combined potable water and hot water in remote locations, hill stations, hospitals, corporate offices and small-scale buildings and industries.

5. Conclusion

In this research, a novel sustainable solar powered combined desalination and hot water (CDHW) system has been investigated experimentally. Basin water and inner glass surface temperatures have been recorded maximum as 67°C and 54°C at 2 p.m. for 0.03 m water depth and 0.0013 kg/s flow rate. Maximum value of radiative, convective and evaporative heat transfer coefficients are obtained as 6.83, 2.75 and 41.23 W/m²·K, respectively at 2 p.m. for 0.03 m water depth and 0.0013 kg/s flow rate. Maximum daily potable water yield, energy efficiency, exergy efficiency and hot water temperature have been obtained as 5.10 kg/m²·d, 42.39%, 4.45% and 67°C, respectively. CPL of potable water has been found minimum as 0.04073 $/L/m² for 25 y of operating life of system.

It is recommended to install such system at roof of hospitals and buildings, remote islands, and hilly locations. Furthermore, utilization of thermal oils/nanofluids as working fluid and phase change materials may further improve the thermodynamic performance of this system.

Conflict of interest

There is no conflict of interest.

Abbreviations

CDHW	—	Combined desalination and hot water
CPL	—	Cost per litre
CRF	—	Capital recovery factor
DSSS	—	Double slope solar still
ETC	—	Evacuated tube collector
IST	—	Indian standard time
SFF	—	Sinking fund factor
SSSS	—	Single slope solar still

Symbols

A	—	Area, m²
c_p	—	Specific heat, J/kg·K
h_{cw}	—	Convective heat transfer coefficient, W/m²·K
h_{ew}	—	Evaporative heat transfer coefficient, W/m²·K
h_{rw}	—	Radiative heat transfer coefficient, W/m²·K
i	—	Interest rate, %
I_c	—	Intensity of solar radiation, W/m²
$\dot{m}$	—	Flow rate, kg/s
$\dot{m}_{ew}$	—	Hourly productivity, kg/m²·h
N	—	Component expected life, y
P	—	Partial saturated vapor pressure, N/m²
Q	—	Heat transfer rate, W
T	—	Temperature, °C
Z	—	Capital investment, $

Greek

ε	—	Emissivity
ε_{eff}	—	Effective remittances
η_I	—	First law efficiency, %
η_{II}	—	Second law efficiency, %
σ	—	Stefan Boltzmann constant, W/m²·K⁴

Subscripts/Location

a	—	Ambient
b	—	Basin
g	—	Glass
gi	—	Glass cover inner surface
in	—	Input
p	—	Projected
sp	—	Serpentine
ss	—	Solar still
sw	—	Still water
u	—	Utilized
w	—	Water
1	—	Thermocouple for solar still inlet temperature
2	—	Thermocouple for water basin temperature
3	—	Thermocouple for basin water temperature
4	—	Thermocouple for inner glass temperature
5	—	Thermocouple for solar still outlet temperature

References

[1] S.K. Sansaniwal, V. Sharma, J. Mathur, Energy and exergy analyses of various typical solar energy applications: a comprehensive review, Renewable Sustainable Energy Rev., 82 (2018) 1576–1601.

[2] A.E. Kabeel, Z.M. Omara, F.A. Essa, A.S. Abdullah, Solar still with condenser–a detailed review, Renewable Sustainable Energy Rev., 59 (2016) 839–857.

[3] M.W. Shahzad, M. Burhan, L. Ang, K.C. Ng, Energy-water environment nexus underpinning future desalination sustainability, Desalination, 413 (2017) 52–64.

[4] M.W. Shahzad, K.C. Ng, K. Thu, B.B. Saha, W.G. Chun, Multi effect desalination and adsorption desalination (MEDAD): a hybrid desalination method, Appl. Therm. Eng., 72 (2014) 289–297.

[5] K.C. Ng, K. Thu, S.J. Oh, L. Ang, M.W. Shahzad, A.B. Ismail, Recent developments in thermally-driven seawater desalination: energy efficiency improvement by hybridization of the MED and AD cycles, Desalination, 356 (2015) 255–270.

[6] M.W. Shahzad, K. Thu, Y. Kim, K.C. Ng, An experimental investigation on MEDAD hybrid desalination cycle, Appl. Energy, 148 (2015) 273–281.

[7] R. Kumar, D.B. Singh, A. Dewangan, V.K. Singh, N. Kumar, Performance of evacuated tube solar collector integrated solar desalination unit-a review, Desal. Water Treat., 230 (2021) 92–115.

[8] S. Chhabra, A.S. Verma, A. Gupta, R. Kumar, A. Karnwal, A. Kumar, V. Vashishtha, D.B. Singh, Attempts to raise the solar still outcome: a short review, Mater. Today Proc., 64 (2022) 1375–1379.

[9] M. Chandrashekara, A. Yadav, Water desalination system using solar heat: a review, Renewable Sustainable Energy Rev., 67 (2017) 1308–1330.

[10] A.M. Manokar, D.P. Winston, A.E. Kabeel, S.E. El-Agouz, R. Sathyamurthy, T. Arunkumar, B. Madhu, A. Ahsan, Integrated PV/T solar still – a mini-review, Desalination, 435 (2018) 259–267.
[11] A.K. Singh, D.B. Singh, A. Mallick, Harender, S.K. Sharma, N. Kumar, V.K. Dwivedi, Performance analysis of specially designed single basin passive solar distillers incorporated with novel solar desalting stills: a review, Sol. Energy, 135 (2019) 146–164.
[12] A.K. Tiwari, G.N. Tiwari, Thermal modeling based on solar fraction and experimental study of the annual and seasonal performance of a single slope passive solar still: the effect of water depths, Desalination, 207 (2007) 184–204.
[13] A.E. Kabeel, Z.M. Omara, F.A. Essa, Enhancement of modified solar still integrated with external condenser using nanofluids: an experimental approach, Energy Convers. Manage., 78 (2014) 493–498.
[14] S.W. Sharshir, G. Peng, L. Wu, N. Yang, F.A. Essa, A.H. Elsheikh, S.I.T. Mohamed, A.E. Kabeel, Enhancing the solar still performance using nanofluids and glass cover cooling: experimental study, Appl. Therm. Eng., 113 (2017) 684–693.
[15] S. Shanmugan, F.A. Essa, Experimental study on single slope single basin solar still using TiO_2 nano layer for natural clean water invention, J. Energy Storage, 30 (2020) 101522, doi: 10.1016/j.est.2020.101522.
[16] V. Singh, R. Kumar, R.K. Sharma, S.P. Singh, H. Sinhmar, D.B. Singh, An investigation on effect of variation of mass flow rate and number of collectors on yearly efficiency of single slope solar still by incorporating N similar photovoltaic thermal flat plate collectors, Water Supply, 22 (2022) 5126–5148.
[17] D. Kumar, R.K. Sharma, D.B. Singh, Effect of the variation of a mass-flow-rate and a number of collectors on the performance of an active solar still, Desal. Water Treat., 248 (2022) 1–17.
[18] S.K. Sharma, A. Mallick, D.B. Singh, G.N. Tiwari, Experimental study of solar energy-based water purifier of single-slope type by incorporating a number of similar evacuated tubular collectors, Environ. Sci. Pollut. Res., 29 (2022) 6837–6856.
[19] A. Raturi, D.B. Singh, P.P. Patil, A.K. Sharma, Sensitivity analysis of a solar still of a single slope type included with N similar evacuated tubular collectors having series connection, Desal. Water Treat., 234 (2021) 309–323.
[20] Sandeep, S. Kumar, V.K. Dwivedi, Experimental study on modified single slope single basin active solar still, Desalination, 367 (2015) 69–75.
[21] R.V. Singh, S. Kumar, M.M. Hasan, M.E. Khan, G.N. Tiwari, Performance of a solar still integrated with evacuated tube collector in natural mode, Desalination, 318 (2013) 25–33.
[22] K. Sampathkumar, T.V. Arjunan, P. Senthilkumar, The experimental investigation of a solar still coupled with an evacuated tube collector, Energy Sources Part A, 35 (2013) 261–270.
[23] S. Kumar, A. Dubey, G.N. Tiwari, A solar still augmented with an evacuated tube collector in forced mode, Desalination, 347 (2014) 15–24.
[24] P. Joshi, G.N. Tiwari, Energy matrices, exergo-economic and enviro-economic analysis of an active single slope solar still integrated with a heat exchanger: a comparative study, Desalination, 443 (2018) 85–98.
[25] G.K. Sharma, A. Mallick, R.K. Sharma, R. Dobriyal, N. Kumar, D.B. Singh, An investigation on dissimilarity of mass flow rate and non exergo-enviro-economic parameters for solar still of single slope type integrated with N similar PVT flat plate collectors having series connection, Environ. Sci. Pollut. Res., 29 (2022) 65842–65859.
[26] S.W. Sharshir, A.H. Elsheikh, P. Peng, N. Yang, M.O.A. El-Samadony, A.E. Kabeel, Thermal performance and exergy analysis of solar stills-a review, Renewable Sustainable Energy Rev., 73 (2017) 521–544.
[27] R.K. Yadav, M. Kumar, J. Singh, D.B. Singh, N. Kumar, Effects of the dissimilarity of water depth on energy and exergy efficiencies and productivity of solar energy, Int. J. Exergy, 38 (2022) 333–345.
[28] V.K. Dwivedi, G.N. Tiwari, Comparison of internal heat transfer coefficients in passive solar stills by different thermal models: an experimental validation, Desalination, 246 (2009) 304–318.
[29] T. Rajaseenivasan, K.K. Murugavel, Theoretical and experimental investigation on double basin double slope solar still, Desalination, 319 (2013) 25–32.
[30] T. Elango, K.K. Murugavel, The effect of the water depth on the productivity for single and double basin double slope glass solar stills, Desalination, 359 (2015) 82–91.
[31] D.B. Singh, G.N. Tiwari, I.M. Al-Helal, V.K. Dwivedi, J.K. Yadav, Effect of energy matrices on life cycle cost analysis of passive solar stills, Sol. Energy, 134 (2016) 9–22.
[32] L. Sahota, G.N. Tiwari, Effect of Al_2O_3 nanoparticles on the performance of passive double slope solar still, Sol. Energy, 130 (2016) 260–272.
[33] H.K. Jani, K.V. Modi, Experimental performance evaluation of single basin dual slope solar still with circular and square cross-sectional hollow fins, Sol. Energy, 179 (2019) 186–194.
[34] V.K. Dwivedi, G.N. Tiwari, Experimental validation of thermal model of a double slope active solar still under natural circulation mode, Desalination, 250 (2010) 49–55.
[35] G. Singh, S. Kumar, G.N. Tiwari, Design fabrication and performance evaluation of a hybrid photovoltaic thermal (PVT) double slope active solar still, Desalination, 277 (2011) 399–406.
[36] M.M. Morad, H.A.M. El-Maghawry, K.I. Wasfy, Improving the double slope solar still performance by using flat-plate solar collector and cooling glass cover, Desalination, 373 (2015) 1–9.
[37] D. Kumar, R.K. Sharma, S.K. Sharma, V.K. Dwivedi, S. Tiwari, D.B. Singh, Influence of dissimilarity of water depth on performance of n alike Photovoltaic thermal flat plate collectors included with double slope Solar still: a comparative study, Desal. Water Treat., 273 (2022) 13–33.
[38] M. Fathy, H. Hassan, M.S. Ahmed, Experimental study on the effect of coupling parabolic trough collector with double slope solar still on its performance, Sol. Energy, 163 (2018) 54–61.
[39] K. Mohammadi, H. Taghvaei, E.G. Rad, Experimental investigation of a double slope active solar still: effect of a new heat exchanger design performance, Appl. Therm. Eng., 180 (2020) 115875, doi: 10.1016/j.applthermaleng.2020.115875.
[40] E. Hedayati-Mehdiabadi, F. Sarhaddi, F. Sobhnamayan, Exergy performance evaluation of a basin-type double-slope solar still equipped with phase-change material and PV/T collector, Renewable Energy, 145 (2020) 2409–2425.
[41] G.N. Tiwari, A.K. Mishra, M. Meraj, A. Ahmad, M.E. Khan, Effect of shape of condensing cover on energy and exergy analysis of a PVT-CPC active solar distillation system, Sol. Energy, 205 (2020) 113–125.
[42] D.B. Singh, G.N. Tiwari, Performance analysis of basin type solar stills integrated with N identical photovoltaic thermal (PVT) compound parabolic concentrator (CPC) collectors: a comparative study, Sol. Energy, 142 (2017) 144–158.
[43] A. Raturi, R. Dobriyal, R.K. Sharma, A. Dwivedi, S.P. Singh, D.B. Singh, Sensitivity investigation for solar still of double slope type included with N similar CPC integrated ETC by incorporating yield and efficiency, Desal. Water Treat., 244 (2021) 12–26.
[44] V. Singh, R. Kumar, D.B. Singh, An investigation on effect of dissimilarity of mass flow rate on hourly, daily and annual efficiencies of double slope type solar still included with N similar PVT compound parabolic concentrators, Desal. Water Treat., 246 (2022) 36–53.
[45] E. Deniz, S. Cinar, Energy, exergy, economic and environmental (4E) analysis of a solar desalination system with humidification-dehumidification, Energy Convers. Manage., 126 (2016) 12–19.
[46] N. Rahbar, A. Asadi, E. Fotouhi-Bafghi, Performance evaluation of two solar stills of different geometries: tubular versus triangular: experimental study, numerical simulation, and second law analysis, Desalination, 443 (2018) 44–55.

[47] A.E. Kabeel, G.B. Abdelaziz, S.M.S. El-Said, Experimental investigation of a solar still with composite material heat storage: energy, exergy and economic analysis, J. Cleaner Prod., 231 (2019) 21–34.
[48] H.J. Mosleh, S.J. Mamouri, M.B. Shafii, A.H. Sima, A new desalination system using a combination of heat pipe, evacuated tube and parabolic trough collector, Energy Convers. Manage., 99 (2015) 141–150.
[49] D.B. Singh, Exergo-economic, enviro-economic and productivity analyses of N identical evacuated tubular collectors integrated double slope solar still, Appl. Therm. Eng., 145 (2019) 96–104.
[50] D.B. Singh, D. Kumar, R.K. Yadav, S.K. Sharma, Y. Chaturbedi, N. Kumar, V.K. Dwivedi, An investigation of effect of mass flow rate variation on productivity, exergoeconomic and enviroeconomic parameters of N similar PVTCPCs included with double slope solar still, Desal. Water Treat., 243 (2021) 1–17.
[51] A. Dubey, S. Kumar, A. Arora, Enviro-energy-exergo-economic analysis of ETC augmented double slope solar still with 'N' parallel tubes under forced mode: environmental and economic feasibility, J. Cleaner Prod., 279 (2021) 123859, doi: 10.1016/j.jclepro.2020.123859.
[52] P. Saini, J. Singh, J. Sarkar, Proposal and performance comparison of various solar-driven novel combined cooling, heating and power system topologies, Energy Convers. Manage., 205 (2020) 112342, doi: 10.1016/j.enconman.2019.112342.
[53] P. Saini, J. Singh, J. Sarkar, Thermodynamic, economic and environmental analyses of a novel solar energy driven small-scale combined cooling, heating and power system, Energy Convers. Manage., 226 (2020) 113542, doi: 10.1016/j.enconman.2020.113542.
[54] P. Saini, J. Singh, J. Sarkar, Novel combined desalination, heating and power systems: energy, exergy, economic and environmental assessments, Renewable Sustainable Energy Rev., 151 (2021) 111612, doi: 10.1016/j.rser.2021.111612.